Applied Catalysis A, General 611 (2021) 117978

Contents lists available at ScienceDirect

Applied Catalysis A, General

journal homepage: www.elsevier.com/locate/apcata

Role of chlorides in reactivation of contaminant nickel on fluid catalytic cracking (FCC) catalysts

Corbett Senter [a], Melissa Clough Mastry [b], Claire C. Zhang [c], William J. Maximuck [d], John A. Gladysz [d], Bilge Yilmaz [e,*]

[a] BASF Refinery Catalysts, 11750 Katy Fwy. #120, Houston, TX, 77079, USA
[b] BASF Refinery Catalysts, Can Rabia 3-5, Barcelona, 08017, Spain
[c] BASF, Analytics & Materials Characterization, 25 Middlesex-Essex Tpk., Iselin, NJ 08830, USA
[d] Texas A&M University, Department of Chemistry, College Station, TX, 77843, USA
[e] BASF Refinery Catalysts, 25 Middlesex-Essex Tpk., Iselin, NJ, 08830, USA

ARTICLE INFO

Keywords:
Fluid catalytic cracking
Nickel
Contaminant metals
Chloride
Reactivation

ABSTRACT

Nickel, a common contaminant in crude oil, deposits on Fluid Catalytic Cracking (FCC) catalysts and induces unwanted dehydrogenation reactions. These lead to an increase in hydrogen and coke which inhibits the FCC unit from reaching its optimal operation. Modern catalyst technologies can include nickel passivation strategies to minimize such detrimental effects, and, over time, aging of the nickel on catalyst also diminishes its deleterious activity to some extent; however, reactivation of nickel due to chemical interactions within the FCC unit can retard aging and further penalize the catalytic performance. For the first time, we attempt to demonstrate and characterize the physiochemical and catalytic effects of chloride ions on contaminant nickel in the FCC environment. Equilibrium catalyst (Ecat) samples obtained from industrial FCC units are exposed to chloride ions, and changes in physicochemical characteristics, catalytic selectivity, and the reducibility of nickel are analyzed. These changes indicate the reactivation of nickel and an increase in unwanted dehydrogenation reactions following exposure to chloride ions. Spectroscopic analyses show that the interaction with chloride ions alters the electronic environment of nickel, which makes it easier to be reduced in the FCC riser, and Advanced Cracking Evaluation (ACE) studies show equilibrium catalysts that were exposed to chloride ions gave higher coke and H_2 yields. These results bridge the gap between existing literature and the FCC environment by demonstrating that chloride ions can interact and reactivate nickel contaminant on FCC catalysts.

1. Introduction

Fluid catalytic cracking (FCC) is an important process for the conversion of crude oil into valuable products including fuels, lubricants, and precursors for making other products. This importance is evidenced by the fact that there are more than 430 FCC units worldwide today [1–3]. First used commercially in 1942 in Baton Rouge, Louisiana (USA), the FCC process cracks high molecular weight hydrocarbon chains into lighter hydrocarbons using high temperatures (525−575 °C) and a heterogeneous catalyst [1,4–7]. Until the development of the FCC process, refineries were inefficient at making valuable products such as gasoline and liquefied petroleum gas (LPG); however, the parallel development of the FCC process and a catalyst capable of fluidization and cracking chemistry enabled refineries to upgrade less valuable fractions of crude oil into high-value diesel, gasoline, and LPG products. The FCC catalyst is primarily composed of zeolite-Y (in the form of ultra-stable zeolite Y or USY), which has a high surface area, but also features a matrix used for cracking reactions. The catalytic system can also include additional features such as nickel and/or vanadium passivation technologies and additives to tune product yields or to control emissions.

The catalyst facilitates beta scission reactions and is relatively robust – a necessity for enduring high temperatures and physical stress during operation. Additionally, FCC catalysts are often exposed to metal contaminants, which are typically introduced into the unit via the FCC feed. A common feed contaminant is nickel, which is often introduced with the feed as a nickel (II) porphyrin structure [8,9]. The concentration of nickel in feed varies widely and can be as high as 100 ppm in extreme

* Corresponding author.
E-mail address: bilge.yilmaz@basf.com (B. Yilmaz).

https://doi.org/10.1016/j.apcata.2020.117978
Received 18 August 2020; Received in revised form 16 December 2020; Accepted 17 December 2020
Available online 21 December 2020

cases, although values lower than 25 ppm are more typical [10]. A well-known dehydrogenation catalyst, nickel deposits on FCC catalyst in concentrations ranging up to 19,000 ppm. The deposited nickel induces unwanted dehydrogenation reactions, which lead to an increase in hydrogen and coke yields [11–14]. Excessive amounts of both hydrogen and coke can be problematic for refiners as they push the FCC unit closer to operating limits. For example, increased hydrogen can constrain the FCC unit's downstream compressor, and increased coke can increase the regenerator temperature towards its maximum limit. However, the nickel contaminant becomes less active as it spends more time in the FCC unit. The oxidative environment in the FCC regenerator oxidizes nickel to nickel oxides. This chemical transformation immobilizes the nickel and greatly reduces its dehydrogenation tendency. Interaction of nickel with alumina phases in the catalyst (such as the low surface area crystalline aluminas used for trapping of contaminant nickel in catalysts designed for processing heavier, residue-containing feedstocks) result in various forms of nickel aluminate [15–19]. Once nickel oxides and aluminates are formed, it is important to keep nickel in those states and inhibit its reduction to metallic nickel in the FCC environment.

There is precedence in literature that chloride ions can both mobilize and reactivate nickel oxides. Earlier work shows that NiO on activated carbon reacts with hydrochloric acid (HCl) to form $NiCl_2$, a mobile compound, which can then be further reduced by H_2 to metallic nickel, a more active dehydrogenation catalyst than NiO [16]. Another study shows the same phenomena using platinum, a metal from the same family as nickel, on zeolite that is exposed to HCl and subsequently reduced with H_2. Additionally, a further study observed a redistribution of platinum on the support following the HCl and H_2 reactions [20,21]. Another contribution showed that deactivated Ni-erionite catalyst regained its dehydrogenation activity when treated with solutions of HCl or NH_4Cl [22]. These examples demonstrate that relatively inert NiO can be reactivated for dehydrogenation chemistry and mobilized by exposure to chloride-containing compounds and set a precedence that this might be possible in the FCC environment. Indeed, industrial reports have noted a correlation between increased chloride content and an increase in unwanted hydrogen production, among other issues. While little literature exists concerning chloride interactions with nickel aluminates, nickel in nickel aluminate exists in a +2 oxidation state (as it does in NiO) and has been shown to be difficult to reduce and less active for dehydrogenation chemistry than metallic nickel [18,19]. Thus, it is hypothesized that chloride could lead to a similar reactivation of nickel aluminate for dehydrogenation chemistry.

Interactions of nickel with chloride ions are relevant to the FCC environment as chloride ion sources can enter the FCC both with feed, sometimes a result of insufficient desalting operations, and with fresh catalyst as part of an alumina-based binder used in incorporated catalysts or from the use of chloride-containing precursors/chemicals in catalyst manufacturing [14,23]. The use of the alumina-based binders for incorporated catalysts is needed for particle integrity in order to control the attrition of the final product. Alumina-based binders often contain chloride as a byproduct in its manufacturing. Chloride content in fresh FCC catalyst can be as high as 1.2 wt.%. Chloride sources coming from the feed vary widely. In heavily contaminated feeds, chloride can be as high as 15 ppm. Chloride sources in the feed can react with steam in the FCC to form HCl, while most of the binder-based chloride is released and converted to HCl in the high-temperature, steam partial pressure environment of the FCC regenerator [24–26]. While these chloride contaminants are well known to lead to deposits in the downstream fractionator, fouling in equipment, and having a negative impact on metallurgy, their effect on nickel contaminants in an FCC has never been formally investigated [27].

The work described herein constitutes the first exploration of the effect of chloride ions on nickel contaminants deposited on actual FCC catalysts using simulated FCC conditions. While circulating in an FCC unit, a fraction of catalyst is continuously added and withdrawn. The continual addition and withdrawal of catalyst introduces an age-distribution of catalyst particles in periodically withdrawn samples that are tested and tracked to monitor performance. This age-distributed catalyst sample is commonly called equilibrium catalyst (Ecat). Ecat samples taken from two different industrial FCC units were selected for this study. These samples were selected due to their differing nickel levels, marked as "high" and "low". It is important to note that the Ecat samples chosen for this study originate from catalysts manufactured by the "*in-situ*" manufacturing route. This route differs from conventional catalyst production process in that zeolite is grown in the microsphere after the spray drying step. The zeolite itself acts as the catalyst binder, thus *in-situ* catalysts do not use chloride-containing binders. As a result, there are no chlorides present in fresh catalyst. In addition, the refineries from which these Ecat samples originate did not report any chlorides coming from the feed. Therefore, this study represents the first time these samples are introduced to chlorides. Table 1 shows the total surface area (TSA), zeolite surface area (ZSA), matrix surface area (MSA) and average particle size (APS) of the Ecat samples studied. It is noted that there are slight differences in surface areas and rare earth oxide content between the low and high nickel containing Ecat samples. For the purpose of this study, we note that these would not have a significant effect on the expected outcome based on the experimental design. Because the Ecat samples that fit the desired criteria (similar technology, similar manufacturing route, no additive usage, no previous chloride exposure) are limited and are based on refineries operating around the world at the moment of this experimental design, these samples represent the best compromise between using industrial Ecats and laboratory generated (deactivated) samples. Ecat samples were chosen over lab-deactivated catalyst as these samples provide the best representation of nickel age distribution in the unit, since it is known that the introduction of nickel contaminants in a laboratory can lead to a distribution of nickel which does not mimic what is seen in an actual FCC unit [1]. To this point, extensive research is focused on the attempt to develop methods to minimize these testing artifacts [28]. Thus, performing such a study on Ecat samples provides results most relevant to industrial application.

The Ecat samples chosen for this study were exposed to chloride ions via introduction of gaseous HCl generated by reaction of aqueous HCl with sulfuric acid [29,30]. This procedure is well established in literature for generating HCl. While literature describes the introduction of HCl via liquid solutions as well, such a method was not included in this study, since FCC catalysts are not normally exposed to such liquid media during FCC operation [22]. As a result, they are not designed to withstand this type of liquid interaction; consequently, FCC structural integrity and catalytic performance can be drastically altered by exposure to liquids. The objective of exposure to HCl is to monitor any conversion of oxidized nickel on Ecat into $NiCl_2$ species. A control experiment was also run exposing Ecat to gaseous N_2. Following each introduction of chloride ions or control treatment, each catalyst sample was then exposed to H_2 to mimic the reducing environment of an FCC riser and reduce any nickel chloride species formed to metallic nickel. The effect of each treatment was then studied by evaluating the physical, chemical, structural, and catalytic changes of the catalysts using particle size measurement, surface area measurement, X-Ray Fluorescence (XRF), Scanning Electron Microscopy (SEM), Advanced Cracking Evaluation (ACE), and CO Diffuse Reflectance Infrared Fourier Transform

Table 1
Surface Area and Average Particle Size of Catalyst Samples.

Sample	TSA, m^2/g	MSA, m^2/g	ZSA, m^2/g	APS, μm
High Nickel, Untreated	153	45	108	74
High Nickel, HCl	159	48	111	79
High Nickel, N_2	154	47	107	69
Low Nickel, Untreated	117	37	80	77
Low Nickel, HCl	118	38	80	77
Low Nickel, N_2	132	39	93	79

Spectroscopy (DRIFTS) analyses. The results are presented and discussed below.

2. Experimental

2.1. Treatment of Ecat samples

A round-bottom flask was charged with catalyst (40 g). $HCl_{(g)}$ was produced by dropwise addition of $HCl_{(aq)}$ (12.1 M, *ca.* 1 mL/min) into a Schlenk flask containing a stirred solution of $H_2SO_{4(aq)}$ (100 mL, 18.0 M). The generated $HCl_{(g)}$ flowed into the catalyst-containing flask via a gas dispersion tube with stirring for 1 h at room temperature and then exhausted into a KOH base trap. The mixture was stirred for 1 h at room temperature. The catalyst was dried using a temperature furnace at 100 °C overnight [29,30].

In a control experiment, the same procedure was repeated with a gentle stream of $N_{2(g)}$ (*ca.* 1 L/min) replacing the generated $HCl_{(g)}$. A round-bottom flask was charged with catalyst (40 g). The $N_{2(g)}$ flowed into the catalyst-containing flask via a gas dispersion tube with stirring for 1 h at room temperature and then exhausted into the atmosphere. The mixture was stirred for 1 h at room temperature. The catalyst was dried in a 100 °C furnace overnight.

The reduction process was adapted from a literature procedure [16]. A Fisher-Porter bottle was charged with treated catalyst (40 g). The system was filled with $H_{2(g)}$ and evacuated five times before being pressurized with 75 psig of $H_{2(g)}$. The system was heated to 375 °C, kept at that temperature for 30 min, and subsequently cooled (total time elapsed ca. 2 h).

2.2. Measurement of particle size of catalyst

Particle size is measured according to ASTM D4464-10. Particle size distribution in the range of 2.8–176 micrometers were measured using a Beckman Coulter LS13320 with Universal Liquid Module and Ultrasonic unit. Material is dispersed in water, exposed to a beam of light, and the diffraction pattern of the light is used to determine the distribution of particle size.

2.3. Measurement of surface area of catalyst

Surface area was measured using the Brunauer–Emmett–Teller (BET) method on a Micromeritics TriStar II according to ASTM methods D 3663 and D 4365. BET uses adsorption isotherms to determine material surface area. The sample was pulverized, and outgassing was performed at 250 °C for 4 h. Surface area was measured by N_2 adsorption and desorption.

2.4. Elemental analysis

X-Ray Fluorescence Spectroscopy analyses were performed using a wavelength-dispersive PANalytical PW2400 spectrometer, calibrated by linear regression to data from standards. All samples were prepared by fusion, using a lithium metaborate/lithium tetraborate flux.

2.5. Scanning Electron Microscopy - Energy Dispersive X-ray Spectroscopy (SEM-EDX)

The catalyst samples were mounted in epoxy and polished to an ultra-flat surface and carbon coated using a Denton DV-502A Vacuum Evaporation System. The BEI analysis was conducted on a Hitachi 3400S Environmental Microscope at 15−25 kV. EDX (Energy Dispersive X-Ray Spectroscopy) results were collected at 25 kV on a Bruker Quantax EDS system with Dual 30 mm^2 Silicon Drift Detectors (SDD).

2.6. Image processing for quantitative analyses

ImageJ was used to calculate the circularity of all particles in each sample. A circularity index was calculated per the following equation:

$$Circularity = 4\pi * \frac{Area}{Perimeter^2}$$

A circularity of 1 equals a perfect circle while a circularity of 0 equals a straight line.

2.7. Fluidized catalytic cracking evaluation

Advanced Cracking Evaluation (ACE) is a laboratory-scale FCC testing unit which evaluates the activity and selectivity of FCC catalysts in a fixed-fluidized bed reactor [31,32]. As testing is carried out under fluidized conditions, it is commonly used for evaluating FCC catalysts. Ecat treated by various methods were analyzed on an ACE testing apparatus with the following conditions: Reactor temperature: 532 °C, injector height, 2.125", standard vacuum gasoil feed, variable time on stream method, 1.2 g/min feed rate, 9 g catalyst loading, 575 s catalyst strip time, liquid strip multiplier of 12, 110 °C feed temperature, 116 °C and 177 °C temperature of first and second feedline heater (respectively), and catalyst to oil ratios of 9, 7, 5, and 3. Coke on catalyst is obtained at the end of a run on a LECO unit.

2.8. CO - Diffuse reflectance infrared Fourier transform spectroscopy (DRIFTS)

A recently developed, 3-temperature (3-T) pretreatment CO DRIFTS method was used to characterize the nickel on samples treated with N_2 and HCl [33]. This method, as opposed to traditional CO DRIFTS, is needed due to the presence of other impurities, which can lead to ambiguous CO band assignments. The samples were ground into fine powders and pretreated with 2.4 % H_2/Ar at 200, 400, and 600 °C sequentially for 1 h at each temperature. The samples were cooled to 30 °C then underwent a 30 min exposure to 1% CO/Ar for adsorption and a 30 min desorption in Ar while FTIR data were collected. FTIR characterization was performed on a Thermo Fisher Nicolet iS50 FTIR spectrometer equipped with an MCT detector and a Pike Technology high-temperature environmental chamber with a KBr window. Spectrum collection was performed under diffuse reflection mode. Bands were assigned based on CO interaction with metals of different oxidation states and the change in these band intensities with temperature was recorded, which allows the characterization of nickel reducibility upon different treatments.

3. Results and discussion

Ecat samples were treated with HCl or N_2, reduced by exposure to H_2, and then analyzed by several techniques. XRF, surface area, and particle size distribution of each sample were measured and compared to untreated Ecat as a means of evaluating the effect of each treatment on chemical composition and physical integrity of the catalyst. SEM images were also obtained in order to evaluate changes in catalyst particle shape and nickel distribution across different catalyst particles. An image processing method employing ImageJ was used to quantify differences seen between each SEM image. Changes in the dehydrogenation activity of nickel on Ecat following each treatment method was evaluated using ACE analysis. A standard feed was cracked over a range of catalyst to oil (C/O) ratios with each Ecat. The properties of this standard feed are given in the table below (Table 2).

Hydrogen and coke yields of the Ecat sample are used as a measure for dehydrogenation activity of contaminant nickel. Finally, the oxidation state of nickel, which is hypothesized to be altered by interaction with chloride ions and subsequent reduction, was evaluated by a CO DRIFTS [33]. The results are described herein.

Table 2
Feed properties used in ACE evaluations.

Property	Value	Distillation, °F	Value
Ni, ppm	0.3	Initial boiling point	267
V, ppm	0.2	5%	578
Na, ppm	0.3	10%	632
Fe, ppm	0.1	20%	689
Cu, ppm	0.1	30%	729
S, wt.%	0.74	40%	769
CRC, wt.%	0.26	50%	805
Total N, ppm	978	60%	842
Basic N, ppm	298	70%	883
UOP K	11.9	80%	926
Pour point, °F	102	90%	978
Aniline point, °F	186	95%	1017
Ref. index @ 25 °C	1.5044	Final boiling point	1122
API @ 60 °F	24.19		

3.1. XRF, adsorption, and particle size distribution

Following the treatments described previously, the resulting surface area and chemical composition of the catalysts were analyzed and compared to untreated samples to evaluate how each treatment method influenced the chemical and physical properties of the catalysts. XRF results are shown in Table 3. Aluminum, lanthanum, iron, nickel and vanadium are reported as oxides. These elements (via their respective oxides) are all of interest. Aluminum is present in both the matrix and zeolite phases of the catalyst and plays the key role in cracking in both the zeolitic domain (especially to provide selectivity towards valuable hydrocarbons such as gasoline and LPG) as well as in the matrix domain (especially to crack large molecules in the feed). Alumina phases can also be used for trapping contaminant metals such as nickel. Lanthanum is a rare earth element which stabilizes active cracking sites. Iron is both a contaminant and found in the structural framework of the catalyst. As a contaminant, iron can act as a dehydrogenation catalyst to generate coke and hydrogen but is considered significantly less active than nickel (ca. one-tenth the activity). Vanadium is also a feed contaminant which contributes to coke and hydrogen yields, but it is also considered to be less active in generating coke and hydrogen compared to nickel (ca. one quarter of the dehydrogenation activity). As a result, it is important to track these elements/oxides before and after treatment methods to assess how any change in their amount might affect the reactivity or selectivity of catalyst samples. It is important to note that no other catalyst contaminants known to increase coke and H_2 were present on the catalyst in significant quantities (>50 ppm). For simplicity, they are not included.

Following treatment by either HCl or N_2 and reduction with H_2, both Ecat samples contained amounts of Al_2O_3, La_2O_3, Fe_2O_3, NiO, and V_2O_5 that were within instrumental error of the untreated Ecat samples. This indicates that loss of nickel, vanadium, aluminum, iron or lanthanum does not occur during treatment (as expected) and will not influence coke and hydrogen yields in ACE analyses. It is also worth noting that there are different amounts of iron and vanadium between the high and low nickel samples; however, these differences are small (ca. 1000 pm Fe and 500 ppm V) compared to the difference in nickel (ca. 4000 ppm Ni) between samples. Furthermore, taking into account the much lower dehydrogenation activities of iron (ca. $1/10^{th}$ of Ni) and vanadium (ca. $1/4^{th}$ of Ni), these differences can be "normalized" to much lower levels. When comparing to a 4000 ppm difference in Ni, these small contributions from Fe and V are considered insignificant in this study.

Table 3
XRF Results of Treated and Untreated Ecat Samples.

Sample	Al_2O_3, wt.%	La_2O_3, wt.%	Fe_2O_3, wt.%	NiO, wt.%	V_2O_5, wt.%
High Nickel, Untreated	40.01	3.28	0.86	0.59	0.39
High Nickel, HCl	40.00	3.21	0.81	0.56	0.38
High Nickel, N_2	40.20	3.28	0.81	0.59	0.41
Low Nickel, Untreated	39.69	2.38	1.04	0.08	0.30
Low Nickel, HCl	40.02	2.40	0.99	0.08	0.29
Low Nickel, N_2	40.35	2.45	1.01	0.09	0.33

Table 1 shows the surface area and average particle size (APS) of the Ecat samples before and after each treatment method. These physical parameters are important to monitor, since any change in the structural integrity of the catalyst could influence coke and hydrogen yields, thus clouding any change in nickel reactivity. Neither treatment method resulted in a change in surface area or particle size that was outside of the instrumental error of the original Ecat. This indicates that HCl and N_2 treatment methods do not significantly alter the catalyst structure.

3.2. Scanning electron microscopy and energy dispersive X-ray spectroscopy

Scanning electron microscopy was performed on catalyst samples before and after treatment to understand both the change in nickel distribution and the structural integrity of the catalysts before and after exposure to chloride ions. SEM studies focused on high nickel Ecat, since the low nickel Ecat samples did not contain enough nickel for detection in SEM-EDX (Energy Dispersive X-Ray Spectroscopy).

Fig. 1 shows the SEM back-scattering results for treated and untreated Ecat samples. No fragmentation of particles was observed, and the structural integrity of the catalyst particles was maintained. ImageJ was used to calculate the circularity of each particle. A "circularity index" of 0 to 1 was calculated with 1 indicating a perfect circle and 0 indicating a line. The values were averaged for each treatment method and the results are shown in Table 4. Each catalyst sample had the same circularity index of 0.86, thus confirming that no treatment method was destructive to catalyst integrity and that these treatment methods are an effective way to introduce chloride into the catalyst without influencing the structural integrity of the catalyst particle.

The SEM-EDX images of nickel on catalyst particles were also examined before and after treatment. Fig. 2 shows the SEM images for nickel and aluminum overlaid for high nickel Ecat untreated and treated by N_2 and HCl.

A redistribution of nickel is not apparent from these images; however, this is not surprising given the design of the experiment. The catalysts were not treated in a fluidized environment nor at the high temperatures experienced in an industrial FCC regenerator. As a result, while nickel chlorides can still form, the temperature and lack of fluidization would not be amenable to nickel mobility. A further study of nickel mobility in the presence of chloride ions at conditions closer to that of an FCC unit will be investigated later.

3.3. Catalytic testing results

Changes in the catalytic behavior of nickel-contaminated Ecat following exposure to N_2 or HCl then reduced by H_2 were evaluated using ACE analyses. A standard FCC feed was cracked over a fluidized bed of Ecat at different catalyst-to-oil ratios. Since nickel is a known contaminant that produces hydrogen and coke when present on FCC catalyst, the changes in coke yield and H_2/CH_4 yield ratios during ACE evaluations were compared as a means of assessing nickel activity following different treatment methods.

Fig. 3 shows the coke vs. conversion results from an ACE analysis of the Ecat sample containing high amounts of nickel. The results showed treatment with HCl prior to the reduction step gave roughly a 1 wt.% increase in coke yield at a given conversion level. This result highlights that the introduction of chloride ions leads to increased coke yield. Since coke is a known product of dehydrogenation from nickel contamination and it is hypothesized that chloride ions facilitate activation of nickel contaminants on FCC catalyst, a higher coke yield following HCl

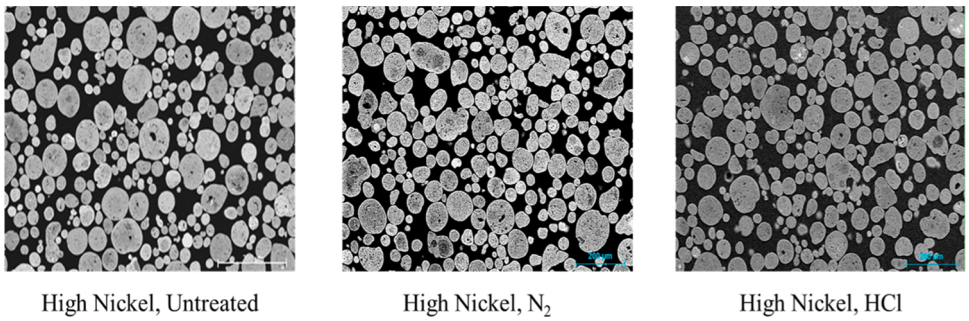

Fig. 1. SEM backscattering images of high nickel Ecat untreated, treated by N_2, and treated by HCl.

Table 4
Circularity of Catalyst Particles Calculated by ImageJ.

Sample	Circularity Index[a]	Number of Particles Analyzed
Untreated	0.86	221
N_2	0.86	234
HCl	0.86	214

[a] See the Experimental Section for the definition of circularity.

exposure suggests the reactivation of nickel by exposure to chloride ions.

Fig. 3 also shows H_2/CH_4 yield ratios as a function of conversion for the high nickel Ecat treated by N_2 and HCl. As with the coke yield, the H_2/CH_4 yield ratio was higher for Ecat exposed to HCl than Ecat exposed to N_2 (~0.08 wt.%/wt.%). The increase in H_2/CH_4 yield ratio with HCl treatment also suggests that there are interactions of chloride ions with nickel which increase the dehydrogenation activity of the nickel contaminants on catalyst.

The average yields at 72.5 % conversion are reported in Table 5. There is a 0.06 wt.%/wt.% and 1.1 wt.% increase in H_2/CH_4 ratios and coke yields, respectively, when the catalyst is treated with HCl as opposed to with N_2. These experiments confirm an average relative increase of 13 % in H_2/CH_4 ratios and 18 % in coke yields for samples exposed to HCl. These increases in H_2/CH_4 and coke are both significant, as the average values of 0.52 and 7.4 for H_2/CH_4 and coke yields following HCl treatment are not within the standard deviation of the H_2/CH_4 and coke values of the samples treated with N_2. Additionally, increases in 13 % and 18 % in H_2/CH_4 and coke would be considered significant by industry standards as well. These increases in H_2/CH_4 and coke seen in Table 5 agree with the trends seen in Fig. 3, thus confirming the increased dehydrogenation which occurs when chloride ions are introduced to the system.

The combination of increased coke and hydrogen yields following exposure to HCl indicates that nickel contaminant on the catalyst is more active, and that chloride ions play a role in reactivating nickel on the catalyst.

Low nickel Ecat samples exposed to N_2 and HCl were also analyzed via ACE. The coke yield vs. conversion plots are shown in Fig. 4. There was a ~0.5 wt.% increase in coke yield following exposure to HCl. However, this increase in coke is not as large as the increase seen (~1

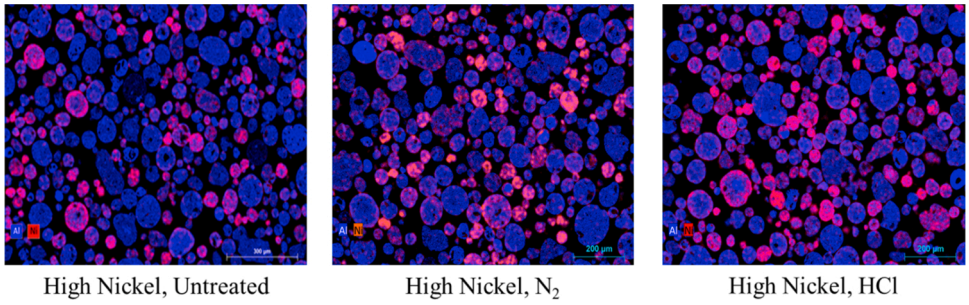

Fig. 2. SEM images of nickel overlaid with aluminum for high nickel Ecat untreated, treated by N_2, and treated by HCl.

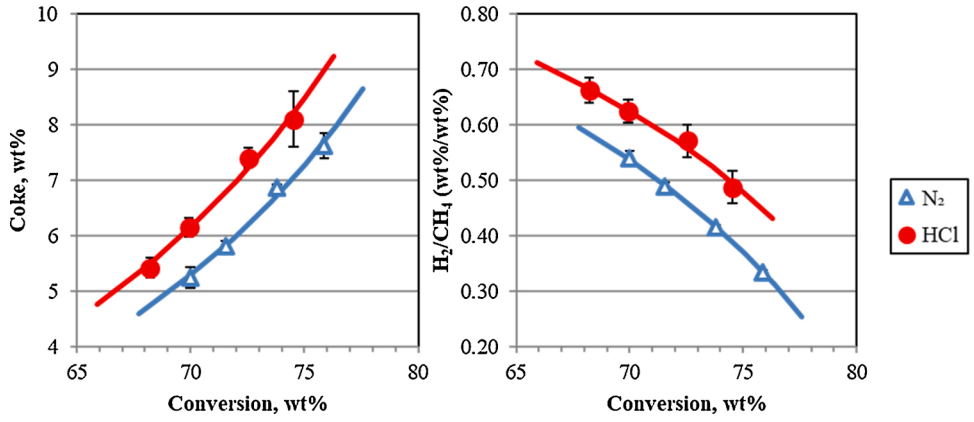

Fig. 3. Coke and H_2/CH_4 vs. conversion for high nickel Ecat sample.

Table 5
Change in H_2/CH_4 ratios and coke yields of Ecat treated by different gaseous methods. High nickel reported at 72.5 % conversion. Low nickel reported at 63.5 % conversion.

		N_2 Treatment	HCl Treatment	% Difference (HCl vs. N_2)
High Nickel	H_2/CH_4	0.46 ± 0.006	0.52 ± 0.04	13
	Coke	6.3 ± 0.1	7.4 ± 0.2	18
Low Nickel	H_2/CH_4	0.19 ± 0.005	0.25 ± 0.008	30
	Coke	3.4 ± 0.05	3.7 ± 0.2	9.8

wt.%) following treatment of the high nickel Ecat sample with HCl. This is expected as there is significantly less nickel present on the Ecat, thus less nickel available for potential reactivation.

Fig. 4 also shows the H_2/CH_4 yield ratio as a function of conversion for the Ecat samples with lower amounts of nickel. As in the high nickel case, there is an increase in H_2/CH_4 following exposure of the catalyst to HCl (+0.05 wt.%/wt.%). However, as was seen with coke yields, this increase in H_2/CH_4 is not as pronounced as seen in the case of catalyst containing high amounts of nickel.

Multiple ACE experiments were run with the low nickel Ecat. The coke yields and H_2/CH_4 yield ratios at constant conversion were averaged and are reported in Table 5. The H_2/CH_4 yield ratios at constant conversion agreed with the trend seen in Fig. 4. There is a 0.06 wt.%/wt.% increase in H_2/CH_4 when HCl is introduced.

The coke yield at constant conversion agreed with the trend shown in Fig. 4. Exposure to HCl leads to a 0.3 wt.% increase in coke compared to exposure to N_2. However, it should be noted, that the increase in coke due to exposure to chlorides is almost within standard deviation of each experimental trial. This is not surprising considering the relatively low amount of nickel present on this catalyst.

3.4. CO-DRIFTS

CO DRIFTS experiments were performed on Ecat samples treated with N_2 or HCl then reduced by H_2. The goal of DRIFTS experiments is to determine the reducibility of the nickel contaminant. Since the Ecat samples contain 0.8–1.0% of iron, the CO adsorption on iron would show overlapped peaks in DRIFTS with the CO adsorbed on Ni. In the literature, CO adsorbed on the bivalent or single valent state of nickel is assigned in the range of 2100−2200 cm^{-1}, CO adsorbed on top of Ni(0) is assigned in 2000−2100 cm^{-1}, and CO adsorbed on Ni(0) can also be found at 1813−2000 cm^{-1} for single-fold or multi-fold bridged adsorption on larger particles [34–37]. CO adsorbed on iron (Fe^{2+}, Fe^0) is reported with similar peak positions [38–40].

In order to differentiate the CO adsorbed on iron and the CO adsorbed on nickel, a sequential CO DRIFTS experiment at 3 temperatures is designed under the pretreatment of hydrogen reduction following the protocol reported in detail elsewhere [33]. In these CO DRIFTS experiments, samples were first treated with H_2 at 200 °C before introducing CO, which allows a partial reduction of iron or nickel to a different degree. The CO was then introduced and adsorbed on samples to reach equilibrium. After CO introduction, the CO was allowed to desorb in argon, and CO DRIFTS data were collected during both CO adsorption and desorption time using FTIR. The FTIR spectra presented in this paper were collected at 30 s of CO desorption, which retain the adsorbed CO on solid and remove all the gas phase CO signals. This process was then repeated at 400 and 600 °C. At each of these temperatures, the reduction degree of nickel and iron is examined by the adsorbed CO FTIR signals. As two different metal oxide materials, nickel oxide and iron oxide are expected to have different reducibilities [41–44]. The 3-temperature trend analysis of reduction allows the separation of nickel and iron when their reducibilities are different. The single-beam FTIR spectrum at 30-second-desorption was processed using the IR background spectrum collected before CO was introduced, which allows the comparison of adsorbed CO bond vibration signals at the different reduction temperatures. From this spectrum, information on the oxidation states of metals on the catalyst were determined based upon CO interaction with these sites [45]. With that, the reducibility of nickel can be isolated from the influence of iron, and the effect of N_2 or HCl treatment on the Ecat samples can be clearly examined.

The CO absorbance spectra of high nickel Ecat treated by gaseous N_2 and HCl are shown in Fig. 5. The CO absorbance spectra of low nickel Ecat samples treated with N_2 and HCl are shown in Fig. 6.

The bands between 1940 cm^{-1} and 2060 cm^{-1} result from CO bound to Ni(0) and Fe(0) species. The 2090 cm^{-1} band is a result of CO bound to Ni(0). The 2120 cm^{-1} band is CO bound to Fe(II) species. The 2140 cm^{-1} and 2160 cm^{-1} bands result from Ni(II) species. Bands were deconvoluted and their areas were integrated at different reduction temperatures in order to determine differences in nickel oxidation state between treatments. The 2090 cm^{-1} and 2120 cm^{-1}, Ni(0) and Fe(II) bands, respectively, have very small areas and it was difficult to infer meaningful information from them in any sample. Thus, the analysis focused on changes in 2140 cm^{-1} and 2160 cm^{-1} band areas (Ni(II)) and the areas of the bands in the 1900-2070 cm^{-1} region (Ni(0) and Fe(0)).

Fig. 7 shows the sum of the integrated areas of the nickel(II) derived 2140 cm^{-1} and 2160 cm^{-1} bands for the high nickel Ecat samples as a function of temperature. The CO adsorption at these two bands is much smaller than the bands in the 1900 – 2070 cm^{-1} region, which supports that the sample contains mostly metallic forms of nickel/iron after reduction. The form of Ni(II) may include NiO or nickel aluminate in the Ecat samples, and possibly $NiCl_2$ in the HCl-treated samples. The contribution to the peaks at 2140 cm^{-1} and 2160 cm^{-1} is believed to come from NiO or nickel aluminate rather than $NiCl_2$ and are indicative

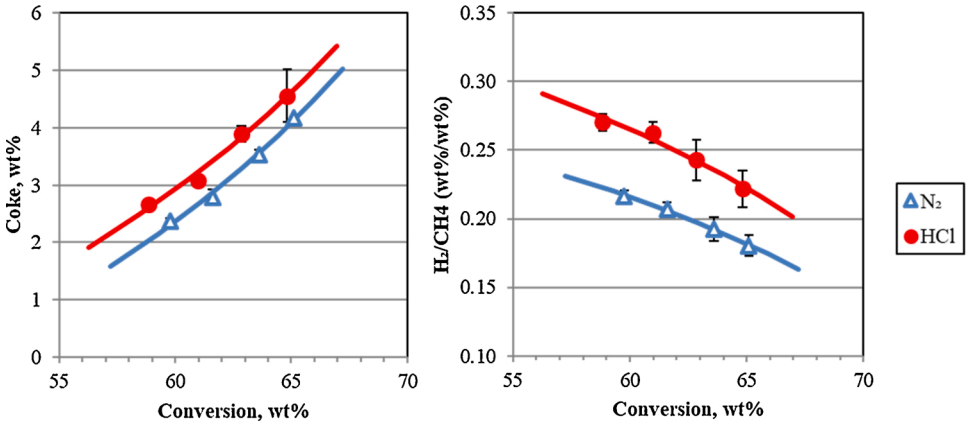

Fig. 4. Coke and H_2/CH_4 vs. conversion yield of low nickel Ecat.

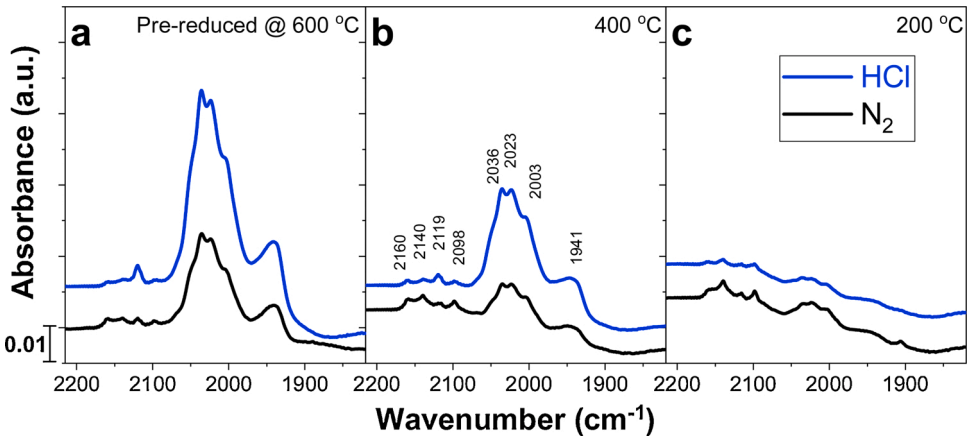

Fig. 5. CO-DRIFTS spectra of high nickel samples treated with gaseous N_2 (lower trace) and HCl (upper trace). Samples are pre-reduced at (L to R) 600 °C, 400 °C, and 200 °C.

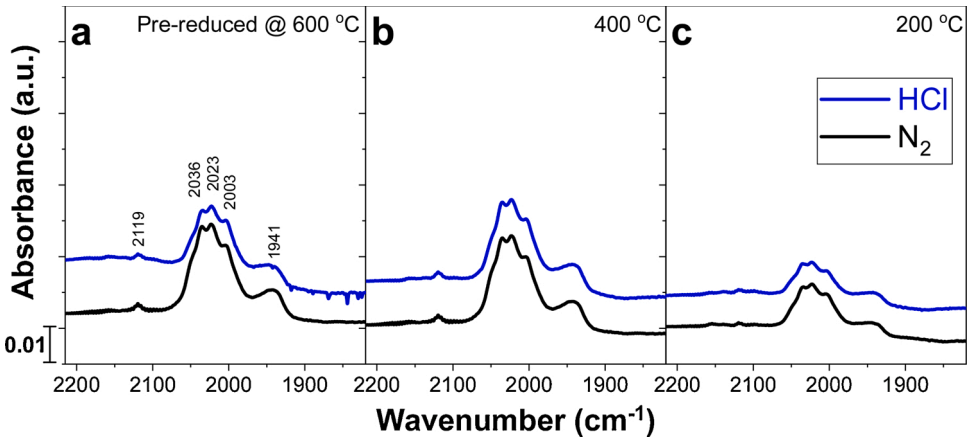

Fig. 6. CO-DRIFTS spectra of low nickel Ecat treated with N_2 (lower trace) and HCl (upper trace).

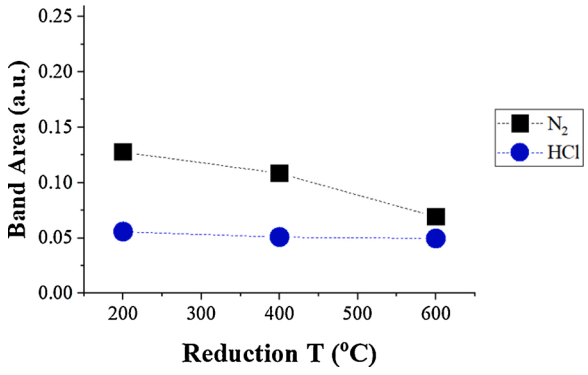

Fig. 7. Area of the 2140 and 2160 cm^{-1} Ni(II)-IR bands of high nickel Ecat as a function of reduction temperature.

of the amount of NiO/nickel aluminate compound (in short, referred to as Ni-O in discussion below) present on the catalyst. These proposed peak assignments can be supported by the observation that the catalyst treated with HCl showed significantly lower band area and, therefore, less Ni-O containing compounds, than the sample treated with N_2. This could indicate that during treatment with HCl, chloride ions reacted with Ni-O, forming $NiCl_2$, which could then be reduced to metallic nickel during the reduction step. Additionally, the N_2 treated sample showed a higher band area at 200 °C and a decrease in this band area with increasing reduction temperature, while the chloride ion treated sample was essentially unchanged, indicating Ni-O remaining on Ecat treated with N_2 is reduced at higher temperatures, while Ecat sample treated with HCl has much less Ni-O remaining. This result suggests different amounts of Ni-O species remain in the Ecat samples under N_2 and HCl treatments, with a higher amount of Ni-O in the N_2-treated Ecat.

The combined band area between 1900–2070 cm^{-1} was also examined. These bands are indicative of both Ni(0) and Fe(0) species; as a result, these combined band areas are discussed for both the high nickel and low nickel catalyst samples to understand whether changes in band area are influenced by changes in Fe(0) or Ni(0) compounds, as the iron levels between the high and low nickel catalysts were similar (within 1200 ppm).

Fig. 8 shows the combined band area of all bands in the 1900–2070 cm^{-1} region for the Ecat samples. It is expected that iron would be reduced before nickel is reduced when exposed to H_2. The formation of Ni(0) will become more obvious as the reduction temperature increases, thus the Ni(0) can be separated from Fe(0) in the CO DRIFTS.

For the low nickel Ecat, as the reduction temperature increases to 400 °C, the bands grow for each sample indicating more Ni(0) and Fe(0) are formed. At 600 °C, important observations can be made. For both low nickel samples, the band area does not increase, which could be an indication that all iron and nickel have been completely reduced to the zero-oxidation state at 400 °C. This result has implications for the analysis of the high nickel sample. The high and low nickel catalyst samples have comparable levels of iron. Thus, a complete reduction of iron in the low nickel Ecat at 400 °C indicates that all iron will be reduced to Fe(0) in the high nickel Ecat at 400 °C as well. Consequently,

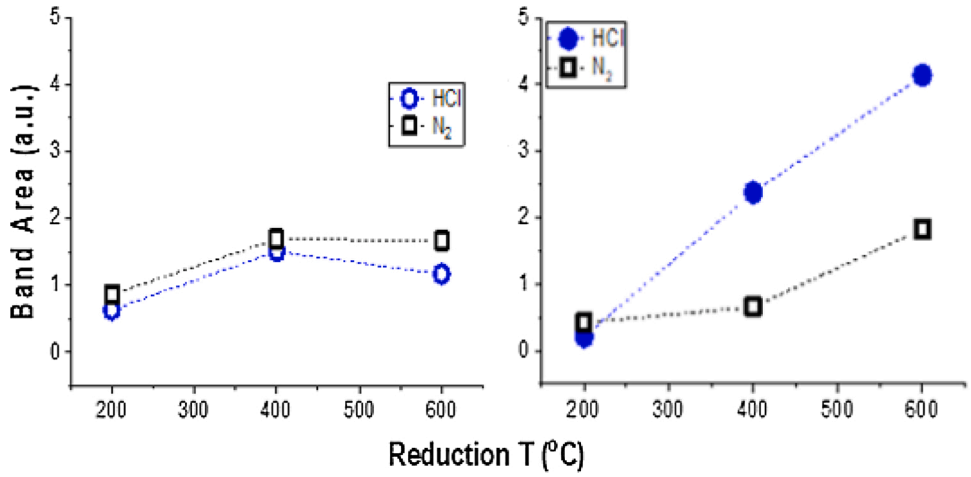

Fig. 8. Sum of IR-band areas for low nickel (L) and high nickel (R) Ecat between 1900 and 2070 cm^{-1} as a function of reduction temperature.

any changes in band area at 600 °C for the high nickel samples can be attributed to a change in the amount of Ni(0).

The combined area of all bands in the 1900–2070 cm^{-1} region for the high nickel catalyst samples can also be seen in Fig. 8. These band areas should reflect the amount of Fe(0) and Ni(0) present. At 200 °C, the area is similar to the low nickel samples, which is an indication that the primary species being observed here is Fe(0) since the nickel levels are very different between the two catalysts. As the temperature increases to 400 °C, the band of the HCl treated sample grows much more rapidly than the N_2 sample. At 600 °C, both high nickel samples show an increase in band area, with the HCl treated sample showing a significantly higher increase than the N_2 treated sample. Having established that the reduction of iron to Fe(0) is completed by 400 °C, this would indicate that the increase in band area at 600 °C is due to a change in Ni(0). This difference in the change in band area would then indicate that the HCl treated sample contains more readily reducible nickel than the N_2 treated sample.

This large increase in Ni(0) formation vs. temperature for Ecat treated with HCl must be reconciled with the fact that its CO adsorbed on Ni-O band at 2140 and 2160 cm^{-1} does not change with a reduction temperature (Fig. 7). One would expect a large increase in Ni(0) to correspond to a drop in Ni(II). An explanation could be that a nickel species not detected in CO DRIFTS is being reduced to Ni(0) at 600 °C in the Ecat treated with HCl. Given the HCl treatment applied, it could be that $NiCl_2$ is present on the Ecat treated by HCl and is not distinguishable in the FTIR spectra studied. As this $NiCl_2$ is exposed to H_2 at 600 °C, it is reduced to Ni(0) which is then visible in the analysis. While the exact mechanism is uncertain, the results show clearly that exposure of Ecat to HCl results in significant differences in the reducibility of nickel compared to exposure to N_2. This further supports the conclusion that differences in ACE yields are a result of a change in the reducibility of nickel, and that chloride ions are playing a major role in this transformation.

4. Conclusions

This work attempts to demonstrate and characterize the physiochemical and catalytic effects of chloride ions on contaminant nickel in the FCC environment for the first time. Additionally, by performing the study on catalyst samples from actual FCC units, the age-distribution of nickel on the catalyst studied is representative of what can be expected in actual operation. It is acknowledged that uncertainties are introduced by using actual FCC Ecat, but the method development work performed in this study has laid the groundwork to perform future studies in more carefully controlled laboratory conditions. Uncertainties which will be addressed in future work include aspects such as the use of catalyst with the same properties and non-Ni contaminants, examination of the effect of different Ni passivators, the effect of Cl contamination on catalyst activity through in depth studies, and using additional techniques to characterize the state of nickel on Ecat.

By studying the change in physicochemical characteristics and catalytic selectivity of FCC catalysts, as well as the reducibility of the nickel on FCC catalyst, clear differences can be seen when catalyst contaminated with nickel is exposed to HCl and then reduced. Catalyst exposed to HCl showed increased coke and H_2 yields and contained less Ni-O bonds. These results bridge the gap between existing literature and the FCC environment by showing that chloride ions can interact with nickel contaminant on FCC catalyst. The interaction results in changes in the electronic environment of nickel, which makes it easier to be reduced in the FCC riser. This reduced nickel poses a significant problem to refineries since it is an active dehydrogenation catalyst which produces undesirable coke and H_2. This increased coke and H_2 brings the FCC unit closer to its operational constraints and inhibits the refinery from reaching the full potential of this important unit operation. The results from this study enable catalyst manufacturers and refiners to further optimize catalyst design and selection as well as operational strategies to limit H_2 and coke from nickel contaminants.

Declaration of Competing Interest

The authors report no declarations of competing interest.

CRediT authorship contribution statement

Corbett Senter: Conceptualization, Methodology, Data curation, Visualization, Writing - original draft, Writing - review & editing, Project administration. **Melissa Clough Mastry:** Conceptualization, Methodology, Data curation, Visualization, Writing - review & editing. **Claire C. Zhang:** Data curation, Visualization, Investigation, Writing - review & editing. **William J. Maximuck:** Data curation, Visualization, Investigation, Writing - review & editing. **John A. Gladysz:** Data curation, Visualization, Investigation, Writing - review & editing. **Bilge Yilmaz:** Conceptualization, Methodology, Supervision, Funding acquisition, Writing - original draft, Writing - review & editing.

References

[1] S.S. Pan, L.T.X. Lin, V. Komvokis, A. Spann, M. Clough, B. Yilmaz, Am. Chem. Soc. 1213 (2015) 3–18.
[2] A.A. Avidan, M. Edwards, H. Owen, Oil Gas J. 88 (1990) 33–58.
[3] E.T.C. Vogt, B.M. Weckhuysen, Chem. Soc. Rev. 44 (2015) 7342–7370.
[4] M. Clough, J.C. Pope, L.T.X. Lin, V. Komvokis, S.S. Pan, B. Yilmaz, Microporous Mesoporous Mater. 254 (2017) 45–58.

[5] NACS, North Am. Catal. Soc. (2003).
[6] V. Blay, B. Louis, R. Miravalles, T. Yokoi, K.A. Peccatiello, M. Clough, B. Yilmaz, ACS Catal. 7 (2017) 6542–6566.
[7] S. Reza, Fluid Catalytic Cracking Handbook, Elsevier, 2012, p. 3.
[8] J.G. Reynolds, Petrol. Sci. Technol. 19 (2001) 979–1007.
[9] G. Busca, P. Riani, G. Garbarino, G. Ziemacki, L. Gambino, E. Montanari, R. Millini, Appl. Catal. A Gen. 486 (2014) 176–186.
[10] P. Bai, U.J. Etim, Z. Yan, S. Mintova, Z. Zhang, Z. Zhong, X. Gao, Catal. Rev. (2018) 333–405.
[11] H.S. Cerqueira, G. Caeiro, L. Costa, F. Ramôa Ribeiro, J. Mol. Catal. A Chem. 292 (2008) 1–13.
[12] M. Xu, X. Liu, R.J. Madon, J. Catal. 207 (2002) 237–246.
[13] F.V. Pinto, A.S. Escobar, B.G. de Oliveira, Y.L. Lam, H.S. Cerqueira, B. Louis, J. P. Tessonnier, D.S. Su, M.M. Pereira, Appl. Catal. A Gen. 388 (2010) 15–21.
[14] M. Gambino, M. Veselý, M. Filez, R. Oord, D. Ferreira Sanchez, D. Grolimund, N. Nesterenko, D. Minoux, M. Maquet, F. Meirer, B.M. Weckhuysen, Angew. Chemie Int. Ed. 10 (2020) 3922–3927.
[15] E.L. Kugler, D.P. Leta, J. Catal. 109 (1988) 387–395.
[16] Y. Ohtsuka, J. Mol. Catal. 54 (1989) 225–235.
[17] V. Cadet, F. Raatz, J. Lynch, C. Marcilly, Appl. Catal. 68 (1991) 263–275.
[18] V. Cadet, F. Raatz, J. Lynch, C. Marcilly, Appl. Catal. 1 (1991) 263–275.
[19] G.L. Woolery, M.D. Farnos, A.R. Quinones, Structure activity correlations on Ni-contaminated FCC, in: National American Chemical Society Meeting, Web, 1996.
[20] K. Foger, H. Jaeger, J. Catal. 92 (1985) 64–78.
[21] K. Foger, H. Jaeger, Appl. Catal. 56 (1989) 137–147.
[22] N.Y. Chen, Chem. Abstr. 77 (1972) 118822.
[23] M. Melin, C. Baillie, G. McElhiney, Petrol. Technol. Q. Q4 (2009) 135–139.
[24] K.H.J. Buschow, R.C. John, W.C. Fort, Encyclopedia of Materials, Elsevier Science, 2001, pp. 6840–6842.
[25] M.R. Gray, P.E. Eaton, T. Le, Pet. Sci. Technol. 16 (2008) 1924–1933.
[26] H. Kaur, P. Eaton, M.R. Gray, Pet. Sci. Technol. 10 (2012) 993–1003.
[27] D.O. Martin, R.O. Allen, Pet. Technol. Q. 6 (2001) 41–45.
[28] D. Wallenstein, D. Farmer, J. Knoell, C.M. Fougret, S. Brandt, Appl. Catal. A Gen. 462-463 (2013) 91–99.
[29] R.N. Maxson, Inorg. Synth. 1 (1939) 147–149.
[30] G. Brauer, Handbuch Der Präparativen Anorganischen Chemie, Eugen Göbel Book Printing Company, Tübingen, Germany, 1954.
[31] Kayser, J.C. Versatile Fluidized Bed Reactor. US Pat. 6,069,012. 1998.
[32] C.P. Kelkar, M. Xu, R.J. Madon, Ind. Eng. Chem. Res. 42 (2003) 426–433.
[33] C.C. Zhang, J. Shi, S. Hartlaub, J.P. Palamara, I. Petrovic, B. Yilmaz, Catal. Commun. 150 (2021) 106273, https://doi.org/10.1016/j.catcom.2020.106273.
[34] J.T. Yates, C.W. Garland, J. Phys. Chem. 4 (1961) 617–624.
[35] L. Kubelková, J. Nováková, N.I. Jaeger, G. Schulz-Ekloff, Appl. Catal. A Gen. 1 (1993) 87–101.
[36] S. Fujita, M. Nakamura, T. Doi, N. Takezawa, Appl. Catal. A Gen. 1 (1993) 87–100.
[37] G. Garbarino, E. Finocchio, A. Lagazzo, I. Valsamakis, P. Riani, V.S. Escribano, G. Busca, Appl. Catal. B (2014) 813–826.
[38] A. Zecchina, F. Geobaldo, C. Lamberti, S. Bordiga, G. Turnes Palomino, C.O. Arean, Catal. Lett. 1–2 (1996) 25–33.
[39] T. Wadayama, K. Kubo, T. Yamashita, T. Tanabe, A. Hatta, J. Phys. Chem. B 16 (2003) 3768–3773.
[40] R. Kefirov, E. Ivanova, K. Hadjiivanov, S. Dzwigaj, M. Che, Catal. Lett. 3–4 (2008) 209–214.
[41] D. Wagner, O. Devisme, F. Patisson, D.A. Ablitzer, Laboratory Study of the Reduction of Iron Oxides by Hydrogen, in: 2006 TMS Fall Extraction and Processing Division: Sohn International Symposium, 2, 2008.
[42] A. Pineau, N. Kanari, I. Gaballah, Thermochim. Acta 1 (2006) 89–100.
[43] A. Pineau, N. Kanari, I. Gaballah, Thermochim. Acta 2 (2007) 75–88.
[44] R. Chatterjee, S. Banerjee, S. Banerjee, D. Ghosh, Trans. Indian Inst. Met. 3 (2012) 265–273.
[45] S.R. Bare, M.E. Charochak, S.D. Kelly, B. Lai, J. Wang, Y.K. Chen-Wiegart, ChemCatChem 6 (2014) 1427–1437.